Growth of Bilayer Graphene on Insulating Substrates

Zheng Yan,[†] Zhiwei Peng,[†] Zhengzong Sun,[†] Jun Yao,[‡] Yu Zhu,[†] Zheng Liu,[§] Pulickel M. Ajayan,[†,§,⊥] and James M. Tour[†,§,⊥,*]

[†]Department of Chemistry, [‡]Applied Physics Program through the Department of Bioengineering, [§]Department of Mechanical Engineering and Materials Science, and the [⊥]Richard E. Smalley Institute for Nanoscale Science and Technology, Rice University, 6100 Main Street, Houston, Texas 77005, United States

ABSTRACT Here we demonstrate a general transfer-free method to directly grow large areas of uniform bilayer graphene on insulating substrates (SiO_2, h-BN, Si_3N_4, and Al_2O_3) from solid carbon sources such as films of poly(2-phenylpropyl)methysiloxane, poly(methyl methacrylate), polystyrene, and poly(acrylonitrile-*co*-butadiene-*co*-styrene), the latter leading to N-doped bilayer graphene due to its inherent nitrogen content. Alternatively, the carbon feeds can be prepared from a self-assembled monolayer of butyltriethoxysilane atop a SiO_2 layer. The carbon feedstocks were deposited on the insulating substrates and then caped with a layer of nickel. At 1000 °C, under low pressure and a reducing atmosphere, the carbon source was transformed into a bilayer graphene film on the insulating substrates. The Ni layer was removed by dissolution, affording the bilayer graphene directly on the insulator with no traces of polymer left from a transfer step. The bilayer nature of as-grown samples was demonstrated by I_G/I_{2D} Raman mapping, the statistics of the full-width at half-maximum of the Raman 2D peak, the selected area electron diffraction patterns over a large area, and randomly imaged graphene edges by high-resolution transmission electron microscopy.

KEYWORDS: bilayer graphene · solid carbon sources · self-assembled monolayers · transfer-free

Since its first isolation in 2004, graphene has garnered enormous interest because of its promising electronic applications.[1−4] Unlike monolayer graphene, AB-stacked (Bernal) bilayer graphene has a tunable band gap, and twisted bilayer graphene has angle-dependent electronic properties, thereby being more attractive for many electronic and optical device applications.[5,6] For such applications, uniform-thickness and large-size bilayer graphene films on insulating substrates are desirable. However, the present growth methods need an additional lift-off step to transfer graphene from the metal catalyst surfaces to the insulating substrates, such as in chemical vapor deposition (CVD) and solid carbon source synthesis methods,[7−13] or they have difficulty yielding uniform bilayer graphene films directly on insulating substrates, as in epitaxial growth methods from SiC.[14−19] Pristine monolayer graphene is a semimetal and demonstrates zero band gap electronic structure, limiting its electronic and optical applications. Progress has been made in opening the band gap of graphene, including using special substrates or defining nanoscale graphene ribbons.[20−22] Another method to modify the bandgap structure of graphene is to periodically replace the carbon atoms in the graphene matrix with heteroatoms such as nitrogen and boron.[10] Recent discoveries demonstrate that a widely tunable bandgap can be realized in bilayer graphene[5] and bilayer graphene−boron nitride (BN) heterostructures,[23] which opens a new door for applications of graphene in electronic and optical devices. Here we demonstrate a general transfer-free method to directly grow large areas of uniform bilayer graphene on insulating substrates (SiO_2, h-BN, Si_3N_4, and Al_2O_3) from solid carbon sources such as films of poly(2-phenylpropyl)methysiloxane (PPMS), poly(methyl methacrylate) (PMMA), polystyrene (PS), and poly(acrylonitrile-*co*-butadiene-*co*-styrene) (ABS), the latter leading to N-doped bilayer graphene due to its inherent nitrogen content. Alternatively, the carbon feeds can be prepared from a self-assembled monolayer (SAM) of butyltriethoxysilane atop a SiO_2 layer. The carbon feedstocks were deposited on the insulating substrates and then caped with a layer of nickel. At 1000 °C, under low pressure and a reducing atmosphere, the carbon source was transformed into a bilayer graphene film on the insulating substrates. The Ni layer was removed by dissolution, affording the bilayer graphene directly on the insulator with no traces of polymer left from a transfer step.

In the present work, the scheme of direct growth of bilayer graphene on insulating substrates is shown in Figure 1a. Here, a heavily doped Si wafer coated with a 500 nm-thick SiO_2 layer (SiO_2/Si) was used as the insulating substrate while PPMS was used as the carbon source. The SiO_2/Si wafer was cleaned with oxygen-plasma and piranha

* Address correspondence to tour@rice.edu.

Received for review July 26, 2011 and accepted September 2, 2011.

Published online September 02, 2011
10.1021/nn202829y

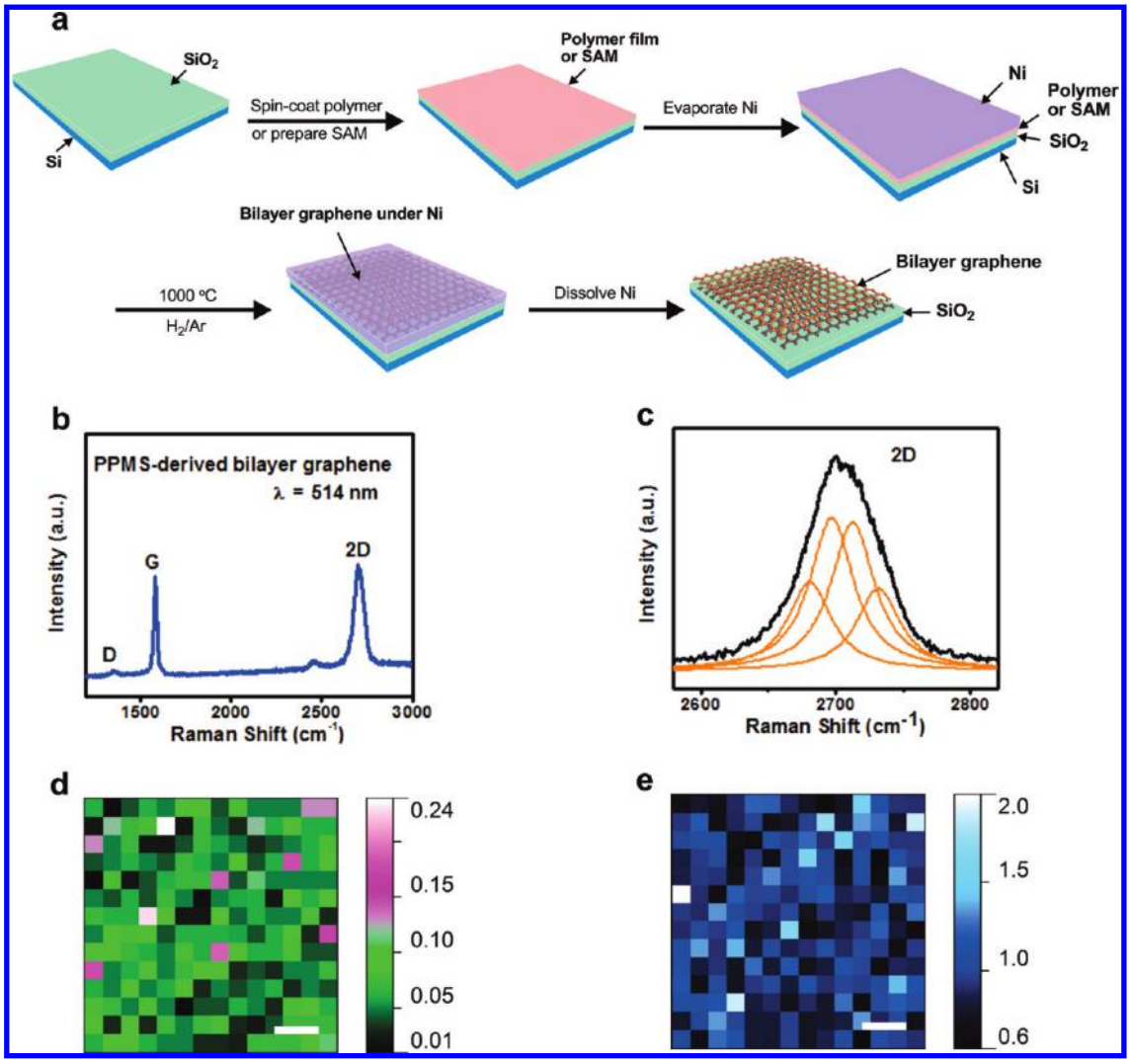

Figure 1. Synthetic protocol and spectroscopic analysis of bilayer graphene. (a) Bilayer graphene is derived from polymers or SAMs on SiO_2/Si substrates by annealing the sample in an H_2/Ar atmosphere at 1000 °C for 15 min. (b) Raman spectrum (514 nm excitation) of bilayer graphene derived from PPMS. See text for details. (c) Bilayered 2D peaks were split into four components: $2D_{1B}$, $2D_{1A}$, $2D_{2A}$, $2D_{2B}$ (yellow peaks, from left to right).[24,25] (d, e) Two-dimensional Raman (514 nm) mapping of the bilayer graphene film (112 × 112 μm^2). The color gradient bar to the right of each map represents the D/G peak ratio (d) or G/2D peak ratio (e) showing ~90% bilayer coverage. The scale bars in d and e are 20 μm.

solution (4:1 sulfuric acid−hydrogen peroxide). Then, a PPMS film (~4 nm thick) was deposited on the SiO_2 by spin-coating 200 μL of PPMS solution in toluene (0.1 wt %) at 8000 rpm for 2 min. A 500 nm Ni film was deposited on top of the PPMS film using a thermal evaporator (Edwards Auto 306); the Ni was used as the metal catalyst for graphene formation. At a temperature of 1000 °C for 7 to 20 min, with a reductive gas flow (H_2/Ar) and under low-pressure conditions (~7 Torr) (Figure S2, Supporting Information), a 1 cm^2 homogeneous bilayer of graphene was synthesized between the insulating substrate and the Ni film. Marble's reagent was used to dissolve the Ni layer. The end result was that bilayer graphene was directly synthesized on the insulating surface, eliminating the transfer process. Instead of using a polymer film, a SAM of butyltriethoxysilane was made on the SiO_2. Using the same Ni deposition and growth conditions, a bilayer of graphene was formed. (See Supporting Information for details.)

In this paper, Raman spectroscopy and transmission electron microscopy (TEM) were used to characterize the as-grown graphene. As a simple tool, Raman spectroscopy was generally used to evaluate the quality and identify the number of layers of graphene made by both CVD and solid carbon source methods.[8,10−13] Here, Raman spectroscopy was first used to characterize graphene derived from PPMS on a SiO_2/Si substrate. Figure 1b shows the Raman spectrum of the PPMS-derived graphene, which is characteristic of 10 locations recorded over 0.5 cm^2 of the sample. The two most pronounced peaks in the spectrum are the G peak at ~1580 cm^{-1} and the 2D peak at ~2700 cm^{-1}. The full-width at half-maximum (fwhm) of the 2D peak and the I_G/I_{2D} peak intensity ratio for bilayer graphene

are significantly different from monolayer graphene and few-layer graphene (Figure S3).[11−13,24,25] Figure 1b shows that the fwhm of the 2D peak is about 50 cm^{-1} and the intensities of the G peak and 2D peak are comparable. Furthermore, the 2D peak in Figure 1b displays an asymmetric line shape and can be well-fitted by four components: $2D_{1B}$, $2D_{1A}$, $2D_{2A}$, $2D_{2B}$ (Figure 1c, yellow peaks, from left to right), individually with fwhm of 30 to 35 cm^{-1}. These data indicate that the PPMS-derived graphene is indeed bilayered.[8,10−13,24,25]

The D peak (1350 cm^{-1}) corresponds to defects in the graphene film. Figure 1b shows that the D peak is very low ($I_D/I_G < 0.1$), indicating few defects in the PPMS-derived graphene. The quality of PPMS-derived graphene over the large area was demonstrated by Raman mappings of the D to G peak ratio (Figure 1d). Areas of 112 × 112 μm^2 were investigated. In the green and black regions (Figure 1d), the D/G peak ratio is below 0.1, suggesting that high-quality graphene covers ~95% of the surface.[10] The quality of PPMS-derived graphene was further confirmed by the low sheet resistance of the graphene film, which is ~2000 Ω sq^{-1} by the four-probe method.[10] The uniformity and the coverage of PPMS-derived bilayer graphene were first illustrated by the Raman mappings of the G to 2D peak ratio (Figure 1e) and the statistics of the fwhm of the Raman 2D peak (Figure S4). An area of 112 × 112 μm^2 was investigated, and the bilayer region was identified by areas I_G/I_{2D} valued between 0.7 (ref 8) and 1.3 (ref 12). The blue region in Figure 1e is bilayer graphene, suggesting bilayer coverage of ~90%. Again, in the same investigated region with I_G/I_{2D} Raman mapping, a histogram of the fwhm of the Raman 2D peak was made (Figure S4), and the bilayer region was identified by the fwhm of the 2D peak valued between 45 and 60 cm^{-1} (ref 13). Figure S4 shows ~90% bilayer coverage in the investigated graphene film, correlating with the result estimated by I_G/I_{2D} Raman mapping.

In this paper, TEM was further used to confirm the bilayer nature of the obtained graphene samples. Although, the PPMS-derived graphene does not need to be transferred to another substrate in order to be used in most applications, the graphene film was peeled from the SiO_2/Si^{2+} substrates using buffered oxide etch for TEM measurements (Supporting Information). TEM images of the pristine PPMS-derived graphene and its diffraction pattern are shown in Figure 2. The suspended graphene films on the TEM grids are continuous over a large area, as seen under low-resolution TEM (Figure 2a and b). The SAED pattern in Figure 2c displays the typical hexagonal crystalline structure of graphene. A 5° rotation is found between the two layers, suggesting non-AA or AB-stacked bilayer graphene films. The diffraction analysis over a large area shows ~90% bilayer coverage in the analyzed region with twisted angles having values between 0° and 30°, correlating with that of the I_G/I_{2D} Raman mapping and the statistics of the fwhm of the Raman 2D peak. In the bilayer region, only a small portion (3−5%) appears to be Bernal stacked (Figure S5).[26,27] The layer count on the edges indicates the thickness of this PMMA-derived graphene. The edge in Figure 2d was randomly imaged under TEM, and most is bilayer graphene, which corroborates the Raman data and diffraction data and provides direct evidence that the as-grown graphene is bilayered. Figure S6 is a photograph of PPMS-derived bilayer graphene synthesized on SiO_2/Si^{2+}, showing that the graphene film covered the insulating wafer (0.75 × 0.6 cm^2).

The electrical properties of the obtained graphene were evaluated with back-gated graphene-based field-effect transistor (FET) devices on a 500 nm thick SiO_2 dielectric. The drain−source current was modulated by applying a back gate voltage. Standard electron-beam lithography and lift-off processes were used to define the source and drain electrodes (30 nm thick Au) in the graphene devices. Graphene stripes (10 μm wide) were further defined by oxygen-plasma etching (Supporting Information). Figure S7a and b show the schematic and the SEM image of the as-made device. Typical data for the FET devices are shown in Figure 3a. The PPMS-derived graphene FET shows an ambipolar behavior, which is similar to that of CVD-grown graphene.[6−11] For this particular device, the carrier (hole) mobility estimated from the slope of the conductivity variation with respect to the gate voltage is ~220 $cm^2\ V^{-1}\ s^{-1}$ at room temperature. In the experiments, more than five devices were made, with mobilities of approximately 220, 180, 150, 130, and 120 $cm^2\ V^{-1}\ s^{-1}$ at room temperature.

The top Ni surface was analyzed after the reaction, and it indeed had its own graphene layer. It often appeared by Raman analysis to be a bilayer, though the signal is more difficult to analyze when on metal. Hence, some carbon below the Ni had diffused through the 500 nm thick Ni film and formed a top graphene bilayer (Figure S9). In one case, we treated the top bilayer graphene film with UV-ozone (directed at the top surface of the Ni), thereby destroying the top-bilayer graphene, as verified by Raman analysis (Figure S10). After Ni dissolution, the bottom graphene bilayer was pristine. Hence, this excludes the possibility that the graphene on top of the Ni drops to the bottom surface after the Ni dissolution.

We propose a limited carbon source precipitation process for the growth mechanism of the polymer and SAM-derived bilayer graphene. In the CVD method, the thickness of graphene is difficult to control when using Ni as the substrate due to the continuous supply of carbon and the high solubility of carbon in Ni.[7,9] In our present method, the amount of feed carbon is limited and fixed between the insulating substrate and the Ni film at the start of the experiment. The amount of carbon in the 4 nm thick PPMS film corresponds to ≤20% of the saturated carbon concentration in a

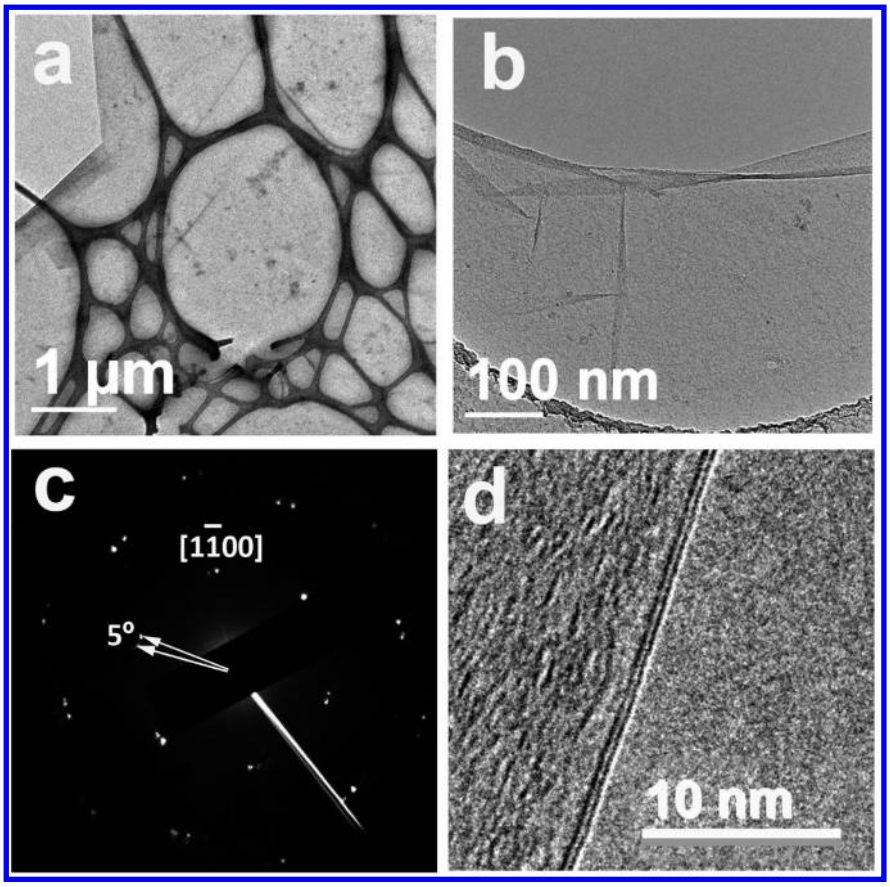

Figure 2. TEM analysis of PPMS-derived bilayer graphene. (a, b) Low-resolution TEM images showing bilayer graphene films suspended on a TEM grid. (c) Hexagonal SAED pattern of the bilayer graphene with a rotation in stacking of 5° between the two layers. (d) HRTEM picture of PPMS-derived graphene edges. The PPMS-derived graphene was two layers thick at random exposed edges.

500 nm thick Ni film at 1000 °C.[28] As illustrated in Figure S8, the 4 nm thick PPMS film decomposed and dissolved into the Ni film during the annealing process. When the sample was removed from the hot-zone of the furnace and rapidly cooled, graphene films precipitated from the Ni. The subsaturated carbon concentration in the Ni film facilitates the growth of bilayer graphene rather than few-layer graphene.[29]

According to the above proposed mechanism, the amount of carbon in PPMS films will affect the graphene growth. Indeed, we controlled the thicknesses of PPMS films by adjusting the concentrations of PPMS-film-forming solutions; the thicknesses of PPMS films were determined by ellipsometry. A 200 μL sample with a concentration of 0.025, 0.1, 0.5, and 1 wt % of PPMS in toluene yielded thicknesses of approximately 1.5, 4, 10, and 20 nm PPMS films, respectively, at spin-coat rates of 8000 rpm. Figure 3b shows that the 4 nm thick PPMS film was the optimal thickness for the growth of high-quality bilayer graphene (the red curve in Figure 3b). When the thickness of the PPMS film was 1.5 nm, the amount of carbon in the related PPMS film is apparently not enough for the formation of graphene (Figure 3b). Too much carbon caused the growth of multilayer graphene with increased defects. Interestingly, the amount of carbon in a ~4 nm thick film of PPMS is very similar to the amount of carbon in four layers of graphene where there is a bilayer below the Ni and an approximate bilayer above the Ni (see Supporting Information for the calculation and Figure S9). When this amount of carbon is exceeded, multilayers and amorphous carbons are formed instead of precisely controlled growth tri- or four-layer graphene. When the amount of carbon is insufficient, discontinuous graphene films are formed (Figure 3b).

The optimized reaction temperature was 1000 °C. A lower temperature (950 °C) leads to a larger D peak in the Raman spectrum (Figure S11a), meaning more defects in the obtained graphene. The highest temperature studied was 1080 °C, at which bilayer graphene with a low D peak was still obtained (Figure S11b).

For the SAM, we used butyltriethoxysilane as the precursor to make a carbon layer on SiO_2 (Supporting Information). Figure 3c shows that the SAM was successfully transformed into bilayer graphene. The sheet resistance was similar to that of PPMS-derived graphene at ~2000 Ω sq^{-1}. Copper was also used as the catalyst for the direct growth of graphene on insulating substrates. Figure S12 shows that copper transformed a 4 nm thick PPMS film into amorphous carbon, while

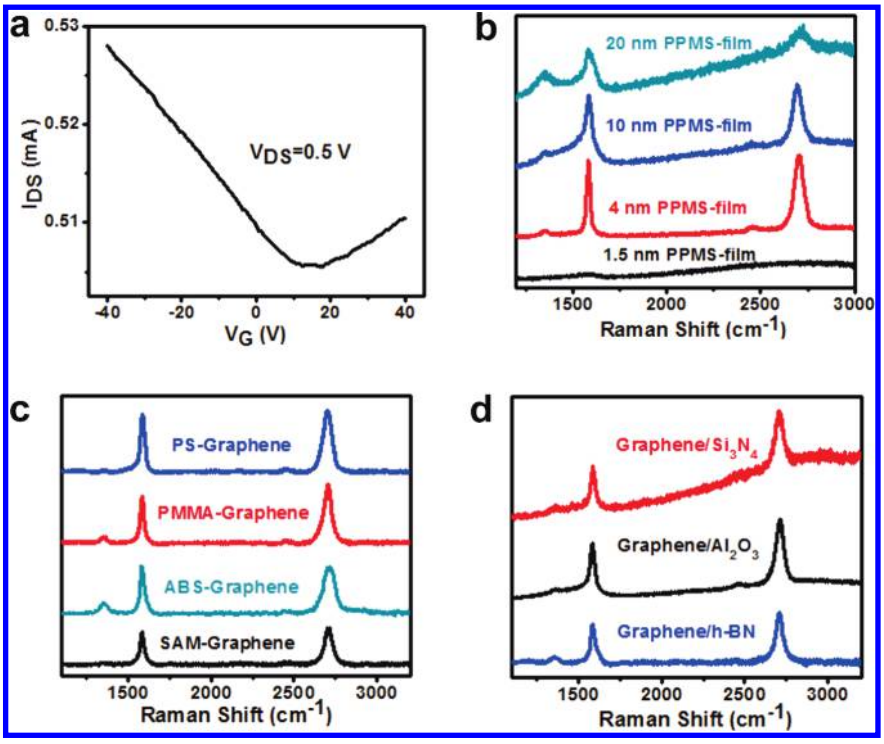

Figure 3. Electrical properties of PPMS-derived graphene and spectroscopic analysis of graphene from different carbon sources and different substrates. (a) Room-temperature $I_{DS}-V_G$ curve from a PPMS-derived bilayer graphene-based back-gated FET device. I_{DS}, drain−source current; V_G, gate voltage; V_{DS}, drain−source voltage. (b) Difference in Raman spectra from PMMS-derived bilayer graphene samples prepared from different thicknesses of the starting PPMS film. (c) Raman spectra of graphene derived from PS, PMMA, ABS, and the SAM made from butyltriethoxysilane. (d) Raman spectra of graphene derived from PPMS on h-BN, Si_3N_4, and Al_2O_3 (sapphire). The baseline has been subtracted from the Raman spectrum of graphene synthesized on h-BN (see Supporting Information Figure S8 for the original data).

the SAM was transformed into multilayer graphene with a large D peak. The growth of graphene on Cu is due to surface catalysis rather than precipitation of carbon from the bulk metal as occurs in Ni.[8]

Other polymers, PS, PMMA, and ABS, were used as carbon feed sources for the direct growth of graphene on insulating substrates. We selected SiO_2/Si (500 nm SiO_2) as the substrate, and the reaction conditions were the same as those used for the PPMS-derived graphene (see Supporting Information for details). The Raman spectra in Figure 3c indicated that all these carbon sources were transformed into bilayer graphene when their thicknesses were fixed at ~4 nm. For PMMA and ABS, the Raman spectrum of the obtained graphene showed slightly larger D peaks (Figure 3c). In ABS, where N-doped bilayer graphene is obtained, a larger D peak is expected due to the broken lattice symmetry.[10] The sheet resistance for PMMA-derived graphene was ~3000 Ω sq^{-1}, and the sheet resistance for ABS-derived graphene was ~5000 Ω sq^{-1}, larger than that of PPMS-derived graphene. The X-ray photoemission spectroscopy (XPS) characterization of ABS-derived graphene demonstrates that ABS films were converted into N-doped graphene, with an N content of 2% (Figure S13). For PS-derived graphene, the low D peak demonstrates the high quality of the obtained graphene film. Its sheet resistance is ~2000 Ω sq^{-1}, similar to that of the PPMS-derived graphene. This can be understood in that PS contains only carbon and hydrogen. The bilayer nature of PS-derived graphene was further confirmed by the SAED pattern and randomly imaged graphene edges (Figure S14).

Using similar conditions, bilayer graphene was also synthesized on several other insulating substrates, thereby underscoring the universality of this direct bilayer graphene growth. The conditions were kept the same as those used for graphene growth on SiO_2 substrates except for replacing the insulating substrates with hexagonal boron nitride (h-BN), Si_3N_4, or Al_2O_3 (sapphire). Large area h-BN was synthesized by CVD of ammonia borane on copper[30] and then transferred onto the SiO_2/Si. After annealing Ni/PPMS/h-BN/SiO_2/Si at 1000 °C for 15 min and dissolving Ni, Raman spectra of the film had G peak and 2D peak signals with comparable intensities, demonstrating the successful synthesis of bilayer graphene on h-BN (Figure 3d). While pure h-BN is nonconductive,[28] the sheet resistance of the obtained graphene/h-BN hybrid film was ~2000 Ω sq^{-1}, measured by the four-probe method. Graphene films were also synthesized on Si_3N_4 or Al_2O_3 as shown in Figure 3d. The sheet resistances of the graphene films on these substrates were both ~2000 Ω sq^{-1}.

In conclusion, we have developed a general route for the direct synthesis of large-size and homogeneous bilayer graphene on various insulating substrates. Most of the bilayer graphene was twisted, including 3−5% in the Bernal region. This method is a new controllable transfer-free route that opens the pathway for scalable bilayer graphene growth with direct compatibility to device construction.

METHODS

The Ni film was deposited *via* an Edwards Auto 306 thermal evaporator. Raman spectroscopy was performed with a Renishaw RE02 Raman microscope using 514 nm laser excitation at room temperature. A 2100F field emission gun transmission electron microscope was used to take the high-resolution TEM images of graphene samples transferred onto a lacey carbon (Ted Pella) or a C-flat TEM grid (Protochips). Electrical characterizations were performed using an Agilent 4155C semiconductor parameter analyzer at room temperature at 10^{-6} Torr. XPS was performed on a PHI Quantera SXM scanning X-ray microprobe with 100 μm beam size and 45° takeoff angle. The thickness of SAMs was determined using an LSE Stokes ellipsometer with a He−Ne laser light source at a λ of 632.8 nm of an angle of incidence of 70°.

Acknowledgment. C. Xiang provided technical assistance. We thank the ONR MURI program (No. 00006766, N00014-09-1-1066), the Lockheed Martin Corporation through the LANCER IV Program, the AFOSR (FA9550-09-1-0581), and the AFOSR through an STTR (FA9550-10-C-0098) with PrivaTran, Inc. for financial support.

Supporting Information Available: Additional materials and methods information, calculations, schemes, Raman, SAED, and XPS spectra. This material is available free of charge *via* the Internet at http://pubs.acs.org.

REFERENCES AND NOTES

1. Novoselov, K. S.; Geim, A. K.; Morozov, S. V.; Jiang, D.; Dubonos, S. V.; Grigorieva, I. V.; Firsov, A. A. Electric Field Effect in Atomically Thin Carbon Films. *Science* **2004**, *306*, 666–669.
2. Geim, A. K.; Novoselov, K. S. The Rise of Graphene. *Nat. Mater.* **2007**, *3*, 183–191.
3. Novoselov, K. S.; Geim, A. K.; Morozov, S. V.; Jiang, D.; Katsnelson, M. I.; Grigorieva, I. V.; Dubonos, S. V.; Firsov, A. A. Two-Dimensional Gas of Massless Dirac Fermions in Graphene. *Nature* **2005**, *438*, 197–200.
4. Ruoff, R. S. Graphene: Calling All Chemists. *Nat. Nanotechnol.* **2008**, *3*, 10–11.
5. Zhang, Y.; Tang, T.; Girit, C.; Hao, Z.; Martin, M.; Zettl, A.; Crommie, M.; Shen, Y. R.; Wang, F. Direct Observation of a Widely Tunable Bandgap in Bilayer Graphene. *Nature* **2009**, *459*, 820–823.
6. Luican, A.; Li, G.; Reina, A.; Kong, J.; Nair, R. R.; Novoselov, K. S.; Geim, A. K.; Andrei, E. Y. Single-Layer Behavior and Its Breakdown in Twisted Graphene Layers. *Phys. Rev. Lett.* **2011**, *106*, 126802.
7. Reina, A.; Jia, X.; Ho, J.; Nezich, D.; Son, H.; Bulovic, V.; Dresselhaus, M. S.; Kong, J. Large Area, Few-Layer Graphene Films on Arbitrary Substrates by Chemical Vapor Deposition. *Nano Lett.* **2009**, *9*, 30–35.
8. Li, X.; Cai, W.; An, J.; Kim, S.; Nah, J.; Yang, D.; Piner, R.; Velamakanni, A.; Jung, I.; Tutuc, E.; *et al*. Large-Area Synthesis of High-Quality and Uniform Graphene Films on Copper Foils. *Science* **2009**, *324*, 1312–1314.
9. Kim, K. S.; Zhao, Y.; Jang, H.; Lee, S. Y.; Kim, J. M.; Kim, J. M.; Kim, K. S.; Ahn, J.; Kim, P.; Choi, J.; *et al*. Large-Scale Pattern Growth of Graphene Films Transparent Electrodes. *Nature* **2009**, *457*, 706–710.
10. Sun, Z.; Yan, Z.; Yao, J.; Beitler, E.; Zhu, Y.; Tour, J. M. Growth of Graphene from Solid Carbon Sources. *Nature* **2010**, *468*, 549–552.
11. Lee, S.; Lee, K.; Zhong, Z. Wafer Scale Homogeneous Bilayer Graphene Films by Chemical Vapor Deposition. *Nano Lett.* **2010**, *10*, 4702–4707.
12. Yan, K.; Peng, H.; Zhou, Y.; Li, H.; Liu, Z. Formation of Bilayer Bernal Graphene: Layer-by-Layer Epitaxy via Chemical Vapor Deposition. *Nano Lett.* **2011**, *11*, 1106–1110.
13. Chen, S.; Cai, W.; Piner, R. D.; Suk, J.; Wu, Y.; Ren, Y.; Kang, J.; Ruoff, R. S. Synthesis and Characterization of Large-Area Graphene and Graphite Films on Commercial Cu-Ni Alloy Foils. *Nano Lett.* DOI: 10.102/nl201699j.
14. Geim, A. K. Graphene: Status and Prospects. *Science* **2009**, *324*, 1530–1534.
15. Berger, C.; Song, Z.; Li, X.; Wu., X.; Brown, N.; Naud, C.; Mayou, D.; Li, T.; Hass, J.; Machenkov, A. N.; *et al*. Electronic Confinement and Coherence in Patterned Epitaxial Graphene. *Science* **2006**, *312*, 1191–1196.
16. Lin, Y.; Dimitrakopoulos, C.; Jenkins, K. A.; Farmer, D. B.; Chiu, H. Y.; Avouris, P. 100-GHz Transistors from Wafer-Scale Epitaxial Graphene. *Science* **2010**, *327*, 662.
17. Berger, C.; Song, Z; Li, T.; Li, X.; Ogbazghi, A. Y.; Feng, R.; Dai, Z.; Marchenkov, A. N.; Conrad, E. H.; *et al*. Ultrathin Epitaxial Graphite: 2D Electron Gas Properties and A Route toward Graphene-Based Nanoelectronics. *J. Phys. Chem. B* **2004**, *108*, 19912–19916.
18. Novoselov, K. S.; Jiang, D.; Schedin, F.; Booth, T. J.; Khotevich, V. V.; Morozov, S. V.; Geim, A. K. Two-Dimensional Atomic Crystals. *Proc. Natl. Acad. Sci. U. S. A.* **2005**, *102*, 10451–10453.
19. Hofrichter, J.; Szafranek, B.; Otto, M.; Echtermeyer, T. J.; Baus, M.; Majerus, A.; Geringer, V.; Ramsteiner, M.; Kurz, H. Synthesis of Graphene on Silicon Dioxide by a Solid Carbon Source. *Nano Lett.* **2010**, *10*, 36–42.
20. Li, X.; Wang, X.; Zhang, L.; Lee, S.; Dai, H. Chemically Derived, Ultrasmooth Graphene Nanoribbon Semiconductor. *Science* **2008**, *319*, 1229–1232.
21. Ohta, T.; Bostwick, A.; Seyller, T.; Horn, K.; Rotenberg, E. Controlling the Electronic Structure of Bilayer Graphene. *Science* **2006**, *313*, 951–954.
22. Zhou, S.; Gweon, G. H.; Fedorov, A. V.; First, P. N.; de Heer, W. A.; Lee, D. H.; Guinea, F.; Neto, A. H.; Lanzara, A. Substrate-induced Bandgap Opening in Epitaxial Graphene. *Nat. Mater.* **2007**, *6*, 770–775.
23. Ramasubramaniam, A. Tunable Band Gaps in Bilayer Graphene-BN Heterostructures. *Nano Lett.* **2011**, *11*, 1070–1075.
24. Ferrari, A. C.; Meyer, J. C.; Scardaci, V.; Casiraghi, C.; Lazzeri, M.; Mauri, F.; Piscanec, S.; Jiang, D.; Novoselov, K. S.; Roth, S.; *et al*. Raman Spectrum of Graphene and Graphene Layers. *Phys. Rev. Lett.* **2006**, *97*, 187401–187404.
25. Luo, Z.; Yu, T.; Shang, J.; Wang, Y.; Lim, S.; Liu, L.; Gurzadyan, G. G.; Shen, Z.; Lin, J. Large-Scale Synthesis of Bi-layer Graphene in Strongly Coupled Stacking Order. *Adv. Funct. Mater.* **2011**, *21*, 911–917.
26. Meyer, J. C.; Geim, A. K.; Katsnelson, M. I.; Novoselov, K. S.; Booth, T. J.; Roth, S. The Structure of Suspended Graphene Sheets. *Nature* **2007**, *446*, 60–63.
27. Hass, J.; Varchon, F.; Millan-Otoya, J. E.; Sprinkle, M.; Sharma, N.; de Heer, W. A.; Berger, C.; First, P. N.; Magaud, L.; Conrad, E. H. Why Multilayer Graphene on 4H-SiC Behaves Like a Single Sheet of Graphene. *Phys. Rev. Lett.* **2008**, *100*, 125504.
28. Singleton M. F.; Nash P. *C-Ni (Carbon-Nickel), Binary Alloy Phase Diagrams*, 2nd ed.; Massalski, T.B., Ed.; Vol. 1, 1990; pp 866−867.
29. Garaj, S.; Hubbard, W.; Golovchenko, J. A. Graphene Synthesis by Ion Implantation. *Appl. Phys. Lett.* **2010**, *97*, 183103.
30. Ci, L.; Song, L.; Jin, C.; Jariwala, D.; Wu, D.; Li, Y.; Srivastava, A; Wang, Z. F.; Storr, K.; Balicas, L.; *et al*. Atomic Layers of Hybridized Boron Nitride and Graphene Domains. *Nat. Mater.* **2010**, *9*, 430–435.